nature portfolio

Peer Review File

Electrically Reconfigurable Polarization Control with Double Tri-layer Black Phosphorus Heterostructures

Corresponding Author: Professor Harry Atwater

This file contains all reviewer reports in order by version, followed by all author rebuttals in order by version.

Version 0:

Reviewer comments:

Reviewer #1

(Remarks to the Author)
The manuscript demonstrates a Fabry-Perot cavity that integrates two cross-aligned black phosphorus layers, enabling electronic access to 86% of the Poincaré sphere. The two BP layers can be independently gated, and the cavity can be tuned across over-coupled coupling and under-coupled coupling. The design is technically sound, and can be of interests for particular readers. However, my main concern lies in the novelty and significance. As pointed out by the authors, gate-tunable anisotropic 2D materials have already been demonstrated for polarization modulation, but the modulation range is limited. It is predictable that stacking two crossed anisotropic 2D materials can enlarge the range, but at the cost of fabrication and device complexity. The two layers work independently, and the whole is no greater than the sum of its parts. Thus, the work is more like a technical reiteration, lacking design innovation or physical insights. Thus, I cannot recommend its publication in NC.

Some other issues:

1. In the introduction, the authors mention "The heterostructure was incorporated into a Fabry-Perot cavity to maximize the exciton-polariton coupling", but there is no related content about exciton-polariton coupling in the following manuscript.

2. How large is the modulation efficiency of the device? What is the proportion of modulated light to the incident light?

3. How does the performance of polarization modulation vary with working wavelengths?

Reviewer #2

(Remarks to the Author)
The paper 'Comprehensively Reconfigurable Polarization Control with Double Tri-layer Black Phosphorus Heterostructures' presents a device concept for a polarization modulator based on anisotropic black phosphorous. The device combines two gate tunable black phosphorous layers in an orthogonal configuration, which allows for two degrees of freedom for controlling polarization. The authors note that simulated results show good coverage of the Poincare sphere assuming a given input polarization. The concept is interesting, and a novel way to achieve compact polarization conversion. However, there are a few key questions and clarifications which need to be addressed;
• The paper freely mixes the use of Poincare sphere and polarization ellipse parameters throughout, which decreases the clarity. The paper could benefit from a brief clarifying sentence to compare the two, especially in comparing the absolute versus difference ellipse measurements used in the theory and the experiment. For instance, are ellipse parameters in Fig 2d and e relative to the lab frame, or to the 45 degree orientation of the polarization with respect to the sample?
• The authors get a range of +40 to -40 degrees in the azimuthal gating map shown in figure 2b. However, as azimuthal ellipse angle typically varies from - 90 to 90 to define all possible linear polarization states on the sphere, it doesn't seem possible to get higher than 50% coverage on the Poincare sphere. Clarifying the above conversions would help clarify this point.
• Several of the plots which pertain to the Poincare sphere, notably Fig 4c and 5b are difficult to understand. It appears that its some form of 3D plot, but its not clear how to interpret them. It looks like a tiny fraction of the sphere is covered looking at the scale. Either the full sphere should be shown, to give appropriate reference for the coverage, or alternatively the authors

could consider doing a scatter plot where the azimuthal and ellipticity angles are plotted as x and y, and the color indicates the doping as shown in the current figure.
• The simulations in 2d and 2e show clear structure in the ellipse parameters which are not observed experimentally. Why is this? Can the non-idealities highlighted in the discussion explain the lack of topography?
• The authors only list the simulated Poincare sphere coverage in the abstract. Either the language should be weakened (aka simulations predict an 86% coverage), or the experimentally demonstrated percentages should be mentioned.
• The objective has angular spread which muddles the input polarization state to the device. How much does this influence the simulated performance of the device? Can this explain some of the discrepancies between theory and experiment?
• Measurements were performed in reference to Au covered PMMA. What are the consequences of this in terms of the absolute reflectance measurements.
• How much does the Poincare sphere coverage decrease if the input polarization is not at exactly 45 degrees to the two flakes?
• How much depolarization is present in the measured experimental data?

Reviewer #3

(Remarks to the Author)
I co-reviewed this manuscript with one of the reviewers who provided the listed reports. This is part of the Nature Communications initiative to facilitate training in peer review and to provide appropriate recognition for Early Career Researchers who co-review manuscripts.

Reviewer #4

(Remarks to the Author)
The manuscript reports a dual-gated, Fabry-Perot cavity device integrating two orthogonally aligned black phosphorus (BP) layers. The authors demonstrate the ability to independently control two degrees of freedom (azimuthal and ellipticity angles) via electrical gating, thereby accessing a significant portion of the Poincaré sphere, at a fixed telecommunication wavelength.
The concept of twisted BP layers for full polarization control has been theoretically explored in Ref. 27. Here, this manuscript provides further experimental validation of a dual-gated, twisted BP device in a metal-mirror Fabry-Perot cavity configuration. The manuscript is generally well-written, and relevant references are properly cited. However, my primary concern is that the experimentally realized range of polarization modulation appears quite limited, falling significantly short of the simulation predictions. Nevertheless, the demonstration of a “2D-control” device based on van der Waals heterostructures remains a notable contribution to the field. I suggest that the authors address the following issues:

1.In the simulations presented in Fig. 1, the accessible polarization coverage is stated to be 86%. However, in Figure 5c, assuming an optimized top gold mirror thickness, the simulated coverage drops to 70%. What is the reason for this discrepancy?
2.The authors only provide the coverage range of Poincaré sphere for the simulations; what is the specific polarization coverage percentage achieved in the actual experiments? Furthermore, in Fig. 5b, there appears to be a significant deviation between the experimental data and the simulated range (15.5 nm top gold mirror thickness). The manuscript lacks a specific analysis for this discrepancy.
3.The device utilizes metal for contacts/mirrors. How do the losses of metal layers influence the modulation of the polarization states?
4.The authors mention that the fabrication process introduces numerous imperfections and contamination, a challenge that is compounded in a 5-stack heterostructure. Given the stochastic nature of the fabrication and the small size of the usable active area, is the reported result reproducible across different devices?
5.What is the modulation speed of the device?
6.The visualization of the polarization state evolution in Fig. 4c and Fig. 5b is somewhat unclear. Are these intended to be three-dimensional plots? A clearer representation would be beneficial.

Version 1:

Reviewer comments:

Reviewer #1

(Remarks to the Author)
The authors have well addressed my concerns, particularly on the novelty. I can now support its publication.

Reviewer #2

(Remarks to the Author)
The authors have appropriately addressed my comments. I believe the work is now appropriate for publication in nature communications.

Reviewer #3

(Remarks to the Author)
I co-reviewed this manuscript with one of the reviewers who provided the listed reports. This is part of the Nature Communications initiative to facilitate training in peer review and to provide appropriate recognition for Early Career Researchers who co-review manuscripts.

Reviewer #4

(Remarks to the Author)
The authors have addressed my concerns and significantly improved the manuscript. I suggest accepting the revised manuscript in its current form.

We thank all reviewers for their suggestions and insights for improving the quality of the work. The detailed point by point responses are listed below. As a note, all reviewer comments are printed in black, our responses are in blue, and text that was added to the revised manuscript and supplementary information are printed in green.

Reviewer #1 (Remarks to the Author):

The manuscript demonstrates a Fabry-Perot cavity that integrates two cross-aligned black phosphorus layers, enabling electronic access to 86% of the Poincaré sphere. The two BP layers can be independently gated, and the cavity can be tuned across over-coupled coupling and under-coupled coupling. The design is technically sound, and can be of interests for particular readers. However, my main concern lies in the novelty and significance. As pointed out by the authors, gate-tunable anisotropic 2D materials have already been demonstrated for polarization modulation, but the modulation range is limited. It is predictable that stacking two crossed anisotropic 2D materials can enlarge the range, but at the cost of fabrication and device complexity. The two layers work independently, and the whole is no greater than the sum of its parts. Thus, the work is more like a technical reiteration, lacking design innovation or physical insights. Thus, I cannot recommend its publication in NC.

We thank the reviewer for their time and input on our manuscript. Below, we have prepared a response addressing the novelty and significance of demonstrating independent, active two-parameter control via excitonic tuning in an optical cavity. The content below has also been paraphrased and added to the manuscript in supplementary notes 12, 17, 18.

Comparison against previous works

As noted by the reviewer, gate-tunable 2D heterostructures for polarization control has been demonstrated before. However, we disagree with the reviewer that the work presented is a technical reiteration. Studies to date involving van der Waals materials employ only one degree of freedom of electronic control[1-3], or focus on passive photodetection (without active gating)[4-6]. Existing devices with two degrees of electronic control to date employ bulk materials that do not exhibit excitonic effects[7,8]. Conversely, our device is the first to demonstrate that dual-gating and two-parameter electronic control is achievable in a 2D heterostructure stack, which is the first step to attaining any arbitrary polarization state with a 2D material device at a single wavelength. A comparison is tabulated in supplementary table 1 for reference:

	Active Material	Material thickness	Accessible parameter space	Tuning method
Ref [4]	BP	40 nm	NIL. Polarimetry measurements	N.A.
Ref [2]	$MoSe_2$	Monolayer	Phase shift	Electronic
Ref [27]	BP	9-14 nm	1D polarization azimuth angle	BP twist angle
Ref [28]	BP	1.59 nm	1D across Poincare sphere	Electronic
Ref [29]	MoS_2	41 nm	1D polarization azimuth angle	Thermo-optic
Ref [8]	Bulk ITO	5 nm	2D across Amplitude & Phase	Electronic
This work	BP	1.59 nm	2D patch on Poincare sphere	Electronic

Supplementary Table 1. Comparison of dual-gated BP device to other similar devices.

Comparison against two single-gated structures

To address the concern that the work is no greater than the sum of its parts, we note that our work is distinctly different from summing the phase/amplitude buildup from two 2D sheets, where the 1D tuning trajectory is increased because the average interaction per round trip within a cavity is doubled. Examples of such a configuration are shown in references [3,27], where the tunable 1D trajectory is merely extended. In this work, we focussed on showing two-dimensional independent control that is necessary for covering any two-parameter space, applying the concept to polarization as an example. Separate independent controls over two orthogonal BP layers result in a multiplicative effect of two differing 1D trajectories, enabling coverage over a two-dimensional parameter space instead.

To further illustrate this point, we simulated an optical setup employing two identical single-gate devices along its optical path (Supplementary Fig. 18a). Assuming that the objective lenses and beam splitter do not affect the polarization state in any way, the second single-gate device is placed with its BP armchair axis oriented to maximally interact with the light reflected from the first device. The S_0 parameter denoting the optical efficiency is shown in supplementary fig. 18b. Due to the need for dual cavities in this setup, the overall reflected efficiency is approximately 20 dB lower than the dual-gated case.

The Poincare sphere coverage is also shown in supplementary fig. 18c. Here, the coverage is about half that of the dual-gated case. This is because the input polarization state into the second device is variable while the AC/ZZ axis of the device itself is fixed. If light is launched parallel to the inactive ZZ axis of the second device, then the second device loses its tunability. We attempted to minimized this by orienting the second device ZZ axis as far from the input polarization as possible, but the tunability still falls off with the input azimuthal angle as $\cos(\psi)$. Therefore, the 2 degrees of freedom in this system are partially coupled, which reduces overall tunability. Incorporation of both BP layers into a single cavity fully decouples the degrees of freedom, which allows a near-full Poincare sphere coverage.

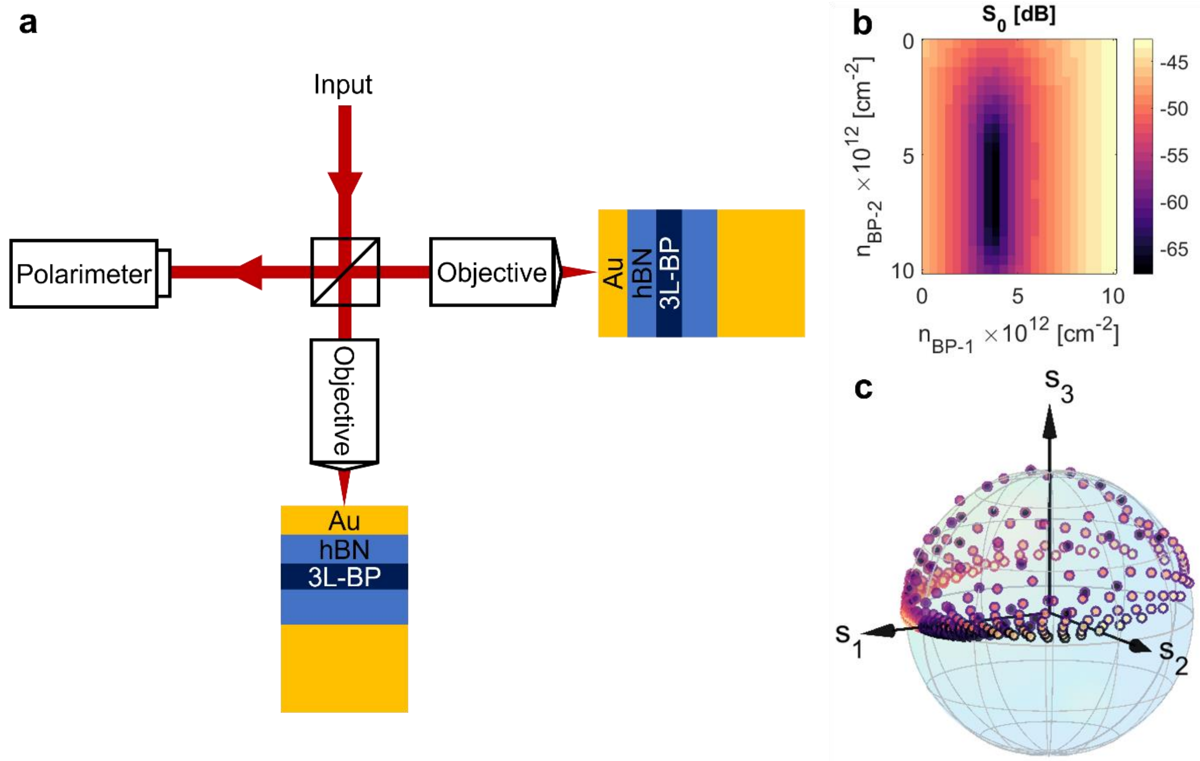

Supplementary Fig. 18. Analysis of cascading two single-gate devices. (**a**) Schematic of optical configuration cascading two single-gate devices. (**b**) S_0 parameter showing decreased optical efficiency due to dual-cavity configuration and beam-splitter for coupling. (**c**) Combined normalized Poincare sphere coverage when gating both devices in concert. Coverage is reduced to less than half of Fig. 1d because of partial coupling between the two degrees of freedom here.

In summary, a configuration employing two single-gate structures suffers from 20 dB poorer optical efficiency, poorer (<50%) polarization coverage due to partial coupling of the degrees of freedom, and a disadvantage in modularity and bulkiness due to the use of two separate devices compared to a single monolithic dual-gate structure demonstrated in this work.

Two-parameter control beyond polarization tuning

We believe our manuscript also provides a framework for future 2D devices for multiple parameter control, beyond just polarization tuning. To illustrate this, we show an additional example below where we cover the phase/amplitude parameter space by replacing one of the 3L-BP layers with graphene (Supplementary Fig. 12). Here, the graphene refractive index model as a function of doping is extensively described in [9]. Since each of the active 2D materials have differing refractive index responses to doping, and their relative placements within the cavity result in differing interactions with the electric field, their respective 1D gating trajectories on the complex reflection plane are inherently different. Combined, this allows for a 2D patch to be accessible via the multiplication of their respective 1D trajectories, which in turn allows the coefficients around the origin to be accessible, implying fully independent amplitude and 360° phase control. Previous similar work on complex modulation was demonstrated by employing a thick layer of indium tin oxide that could build differing charge carrier densities along its top and bottom interfaces.[8] The work presented in the manuscript provides evidence for the experimental viability of two-parameter control via atomically thin heterostructures.

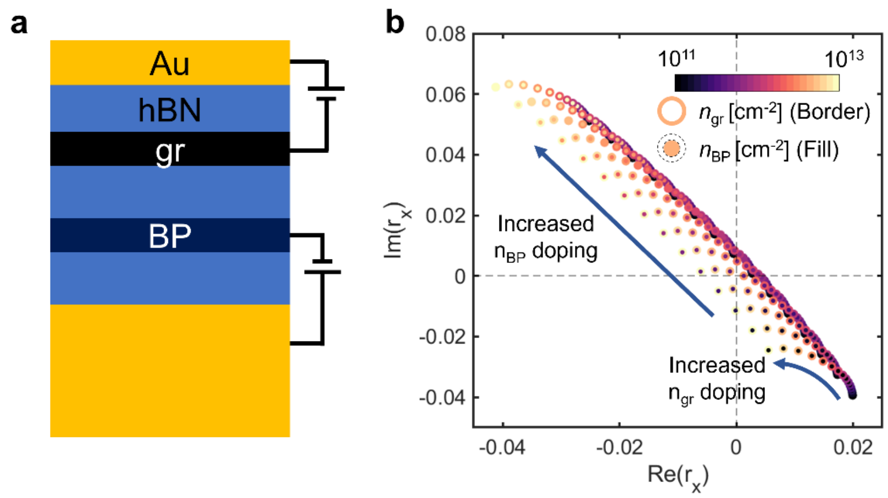

Supplementary Fig. 12. Full independent amplitude and 360° phase modulation device design and simulation. (**a**) Schematic of device. A sheet of p-doped (-0.4eV) graphene (gr) is gated against the top gold contact, while a 3L-BP sheet is gated against the gold back reflector. Linearly polarized light is launched parallel to the AC-axis of the BP layer. (**b**) Simulated complex reflectivity plot of the device at 1502 nm, as a function of carrier densities in the graphene and 3L-BP. Independent control of the carrier densities generates reflection coefficients that pass through and around the origin, indicating independent 360° phase modulation and amplitude modulation.

Additional comments

A further advantage of possessing two electronic degrees of freedom (as opposed to one electronic degree of freedom, together with a non-electronic one), is the decoupling of the degrees of freedom into two fully independent parameters. In the previously cited work of gate-tunable anisotropic 2D materials, both wavelength and gate voltage were used to achieve the required two degrees of freedom for anisotropic phase and amplitude modulation. However, these tuning parameters are inherently coupled - when operating at wavelengths away from the cavity resonance, the anisotropic tuning range afforded by gating drops due to reduced light-matter interaction. This can be seen as a reduction in difference between the solid and dotted lines in Figs. 2a & b at operating wavelengths away from 1479 nm.

Other non-electronic degrees of freedom such as input linear polarization angle faces a similar issue – when input angle is sufficiently tuned away from the active AC axis of the 3L-BP, anisotropic gate tunability drops significantly. Two-parameter control with only one electronic degree of freedom is therefore inherently limited in their dynamic tuning range while requiring the laser wavelength/polarization to be tuned, which is cumbersome for practical applications. Conversely, dual-gated devices can be appropriately designed to have spectrally overlapping resonances in both E_x and E_y. This scheme allows for a single wavelength of operation without compromising on the gating dynamic range or introducing undesired cross-modulation.

To conclude, we hope to have convinced the reviewer with the above analysis that the work is not a reiteration of past studies, but directly improves upon their design to expand the accessible parameter space. Previous similar works employ bulk materials for two-parameter control, or possess tuning ranges limited to 1D trajectories (and therefore suffer from cross-modulation when applied to two-parameter spaces, even if cascaded in series). Here, the method for two-parameter control using atomically thin 2D heterostructures was verified by building a proof-of-concept device focused on polarization control. Our work is therefore the first to demonstrate independent, active two-parameter control via excitonic tuning in an optical cavity.

We included an additional sentence in the 2nd introductory paragraph to compare the dual-gated scheme to other works:

"Further comparisons to past works are included in supplementary notes 17 and 18."

To address the reviewer's comment regarding the summed modulation effects of two separate layers, paragraph 2 of the simulations section has been modified for clarity:

"When gating both BP layers in concert, their respective 1D trajectories are multiplicatively combined, predicting a wide 2D range of output polarization states covering 86% of the Poincaré sphere (Fig. 1d)."

The conclusions paragraph has also been modified to address the implications of experimentally demonstrating a two-parameter control 2D heterostructure:

"This device improved over previous BP polarization modulators by achieving a 2D coverage over the Poincaré sphere through electronic gating alone without the need to change the operating wavelength. Our work is therefore the first to demonstrate independent, active two-parameter control via excitonic tuning in an optical cavity."

"More importantly, our results underscore the potential of 2D heterostructures possessing multiple degrees of freedom imparted by independently controlled gates. To illustrate this further, a device design enabling complex amplitude/360° phase modulation is presented in supplementary note 12."

Some other issues:

1. In the introduction, the authors mention "The heterostructure was incorporated into a Fabry-Perot cavity to maximize the exciton-polariton coupling", but there is no related content about exciton-polariton coupling in the following manuscript.

We thank the reviewer for bringing this to our attention. In order to attain appreciable exciton-polariton coupling, the device must operate in the strong coupling regime given by:[10,11]

$$2g \sim 2\sqrt{\omega_c \Gamma_0} > \kappa, \gamma$$

where g is the coupling strength, ω_c is the exciton frequency, Γ_0 is the radiative decay rate of the exciton (estimated to be 3 ps in this case[12]), κ is the cavity loss rate, and γ is the exciton decay rate. Based on the measurements taken, we determine $2g \approx 28$ meV, $\kappa \approx 59$ meV, and $\gamma \approx 50$ meV, confirming that the device does indeed operate outside of the strong coupling regime.

As such, we've removed the mention of exciton-polariton coupling and instead revised the sentence in the introduction to read:

"The heterostructure was incorporated into a Fabry-Perot cavity to maximize the light-matter interaction of the exciton."

We note it is possible to push the device into the strong coupling regime via several avenues. The coupling strength can be increased by modifying the Fabry-Perot cavity to be plasmonic instead. Exciton linewidth can be reduced by either cooling the system or operating at the edge of a flake[13], and the cavity linewidth can also be reduced by using lossless Bragg reflector mirrors instead.

2. How large is the modulation efficiency of the device? What is the proportion of modulated light to the incident light?

As shown in Fig. 3c, the reflectance from the measured device is about 6%, with most of the losses stemming primarily from dissipative absorption in the gold mirrors. Secondary excitonic absorption also accounts for some optical loss. These losses can be tackled separately:

1) Cavity mirror losses can be reduced by replacing the gold mirrors with lossless Bragg reflectors (DBRs)
2) Excitonic absorption can be reduced by detuning the operating wavelength away from the excitonic resonance, and compensating by increasing the cavity Q in order to accrue sufficient phase and amplitude modulation.[14] This also requires lossless mirrors to achieve high cavity Q

The scheme for high efficiency polarization modulation is described in full in reference [9], where a 75% Poincare sphere coverage is achieved at >20% reflectance. We note that due to the complexity of fabricating such a multi-layer DBR device, we opted to instead demonstrate a low efficiency gold mirror device capable of 2D parameter control.

We have added the following sentence to paragraph 2 of the results section:

"We also note that the optical modulation efficiency reported here is fundamentally limited by the lossy gold mirrors of the Fabry-Perot cavity, but can be improved by replacing them with distributed Bragg reflector mirrors instead as reported in [29]."

3. How does the performance of polarization modulation vary with working wavelengths?

As a response to this question, we performed additional experiments at 1481 nm and included the results in supplementary note 13. We also performed simulations for the critically coupled case showing Poincare sphere coverage as a function of working wavelength:

"While the fabricated device would have a maximum Poincare sphere coverage at the reflectance minimum at 1470 nm, polarization modulation was still observed at 1481 nm (Supplementary Fig. 13a, b). We note that the coverage at 1481 nm is approximately 25% less than at 1470 nm due to the reduction in coupling. Furthermore, we note that the top BP sheet (which primarily controls the output azimuth angle) is better coupled at higher wavelengths.

Conversely, the bottom BP sheet is better coupled at lower wavelengths (as seen in Fig. 4a). This indicates imperfect spectral overlap of the E_x and E_y resonances, which can be fixed by carefully adjusting the thickness of the topmost and bottommost hBN sheets to give equal electric field interaction to both the top and bottom BP sheets.

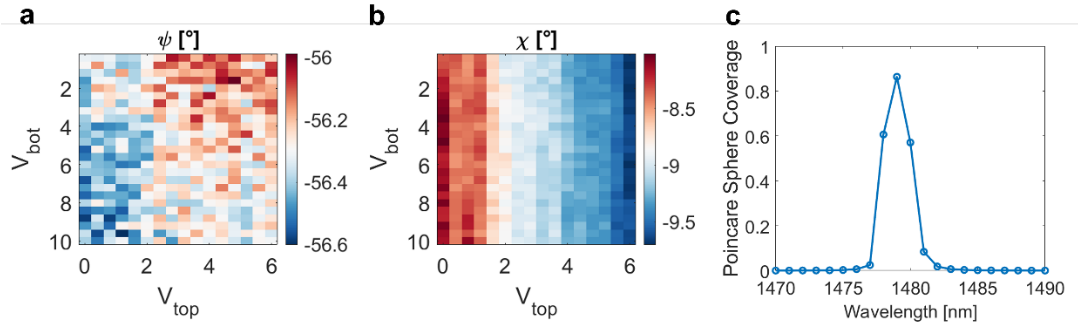

Supplementary Fig. 13. Effect of working wavelength on polarization modulation. (**a** and **b**) Measured azimuthal and elliptical coordinate as a function of top and bottom gating at an operating wavelength of 1481nm. Total polarization coverage here is about 25% less compared to Fig. 4a, b, due to the decreased coupling from operating at the off-resonance wavelength. (**c**) Poincare sphere coverage as a function of working wavelength for the critically coupled case shown in Fig. 1. At the critically coupled regime, the narrow linewidth of the resonance results in a narrow range of operating wavelengths.

For the ideal critically coupled case, the Poincare sphere coverage falls off more sharply than in the experimental under-coupled case (Supplementary Fig. 13c). By comparing against Fig. 2a, b, we see that phase modulation falls off sharply away from the operating wavelength (black dotted line in Fig. 2a, b), and that the amplitude ratio modulation also falls off when moving away from the E_x and E_y minima. This is in agreement with the sharp peak seen in Supplementary Fig. 13c.

We note that the Poincare sphere coverage maximum can be replicated at different wavelengths by modifying the thickness of the hBN dielectric and therefore the Fabry-Perot cavity resonance. The main limiting factor for operating wavelength is the exciton resonance, where modulation drops steadily at sufficiently detuned wavelengths. This is experimentally shown at 1562 nm in supplementary note 9 where a device with a different cavity thickness was made. However, even ~160 nm away from exciton resonance, sufficient spectral overlap between the exciton and cavity exists to measure polarization modulation."

Reviewer #2 (Remarks to the Author):

The paper 'Comprehensively Reconfigurable Polarization Control with Double Tri-layer Black Phosphorus Heterostructures' presents a device concept for a polarization modulator based on anisotropic black phosphorous. The device combines two gate tunable black phosphorous layers in an orthogonal configuration, which allows for two degrees of freedom for controlling polarization. The authors note that simulated results show good coverage of the Poincare sphere assuming a given input polarization. The concept is interesting, and a novel way to achieve compact polarization conversion. However, there are a few key questions and clarifications which need to be addressed;

We thank the reviewer for their positive feedback to our manuscript.

• The paper freely mixes the use of Poincare sphere and polarization ellipse parameters throughout, which decreases the clarity. The paper could benefit from a brief clarifying sentence to compare the two, especially in comparing the absolute versus difference ellipse measurements used in the theory and the experiment. For instance, are ellipse parameters in Fig 2d and e relative to the lab frame, or to the 45 degree orientation of the polarization with respect to the sample?

The choice of using both Poincare sphere and ellipse parameter representations was to present the results in the most understandable way: Poincare sphere representations were used to illustrate the extent of polarization coverage over the orthonormal basis, while ellipse parameters were used to more explicitly show the dependence of polarization on the tuning parameters ($n_{\text{BP-top/bot}}$). To clarify and compare the two, we have included the explicit relations between the ellipse parameters and Stokes parameters in the final line of the Methods section:

"Ellipse parameters are evaluated from the Stokes parameters via the following relations:

$$\psi = \frac{1}{2} atan2\left(\frac{S_2}{S_1}\right), \chi = \frac{1}{2} atan2\left(\frac{S_3}{\sqrt{S_1^2 + S_2^2}}\right),$$

where atan2 is the four-quadrant inverse tangent. Where relevant in the manuscript, Poincare sphere representations were used to illustrate the extent of polarization coverage over the orthonormal basis, while ellipse parameters were used to more explicitly show the dependence of polarization on the tuning parameters ($n_{\text{BP-top/bot}}$)."

We also clarify that the difference ellipse measurements in experiment (Fig. 3d & e) were used to spatially show passive polarization tuning across the device. Namely, the differences in azimuthal/elliptical coordinates between the spatial maps taken at operating wavelengths of 1463 and 1483 nm is plotted out in Fig. 3d & e. This maps out the change in azimuth/elliptical coordinates when varying the input wavelength, which helps to locate areas of polarization responsivity. Once the most polarization-active pixel was identified, the absolute ellipse parameters as a function of gating voltages were mapped out (Fig. 4a & b), in direct comparison to the simulation figures (Fig. 2d & e). To clarify this in-text, we have modified the opening sentence of the Result section's 3rd paragraph to read:

"After determining the optimal input linear polarization angle giving the lowest reflectance minimum, spectral polarization tuning maps were acquired by mapping the area of interest at wavelengths below and above the reflectance dip (1463 nm and 1483 nm respectively), and taking the azimuthal angle differences (Fig. 3d) and elliptical angle differences (Fig. 3e) of these spatial maps at differing operating wavelengths."

Regarding the polarization orientation in Fig. 2d & e, the ellipse parameters in simulations are relative to the device axes shown in the bottom left corner of Fig. 1. Light polarized along the x-direction (parallel to the top 3L-BP's AC axis) has $S_1 = 1$, while light polarized along the lab y-direction (parallel to the bottom 3L-BP's AC axis) has $S_1 = -1$.

The following text has been added to the caption of Fig. 1a for clarity:

"The lab coordinate axes are in the bottom left corner, with the positive x-direction (aligned with the AC axis of the top 3L-BP layer) defining $S_1 = 1$."

Since the 3L-BP flakes are not perfectly orthogonally aligned during fabrication, the polarization basis for experiments was instead aligned against the edges of the gold back reflector which was easier to locate on the optical setup's IR camera. This coordinate system has been included in Fig. 3a for reference:

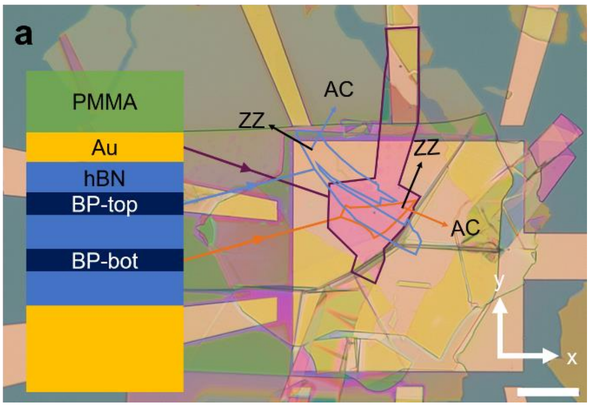

The following text has also been added to the caption for Fig. 3a:

"Coordinate system for polarization basis is shown in the bottom right, with $S_1 = 1$ corresponding to the positive x-direction."

• The authors get a range of +40 to -40 degrees in the azimuthal gating map shown in figure 2b. However, as azimuthal ellipse angle typically varies from - 90 to 90 to define all possible linear polarization states on the sphere, it doesn't seem possible to get higher than 50% coverage on the Poincare sphere. Clarifying the above conversions would help clarify this point.

We thank the reviewer for pointing out the discrepancy between Fig. 1d and 2d. Upon further inspection, it was found that during the conversion of S-parameters to azimuthal coordinates, a regular inverse tangent (atan) was used instead of the proper 4-quadrant inverse tangent (atan2) that is correct for describing the azimuthal/ellipse angles. This corrected the azimuthal closed interval from [-45°, +45°] to [-90°, +90°]. We have therefore amended Fig. 2d accordingly using the 4-quadrant inverse tangent, and it is now consistent with Fig. 1d and 2a.

$$\psi = \frac{1}{2} atan\mathbf{2}\left(\frac{S_2}{S_1}\right)$$

Corrected Fig. 2d:

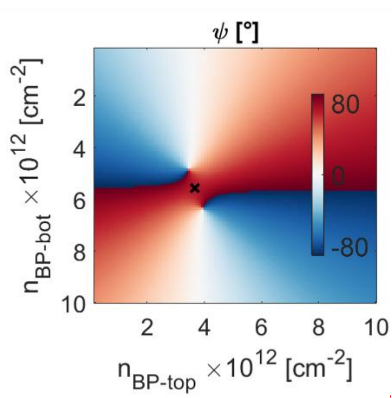

• Several of the plots which pertain to the Poincare sphere, notably Fig 4c and 5b are difficult to understand. It appears that its some form of 3D plot, but its not clear how to interpret them. It looks like a tiny fraction of the sphere is covered looking at the scale. Either the full sphere should be shown, to give appropriate reference for the coverage, or alternatively the authors could consider doing a scatter plot where the azimuthal and ellipticity angles are plotted as x and y, and the color indicates the doping as shown in the current figure.

We fully agree with the reviewer that the plots could be improved and thank them for the suggestion of doing a scatter plot of azimuthal/ellipticity angles. We decided to take their suggestion and modify Fig. 4c and 5b accordingly for clarity.

Fig. 4c:

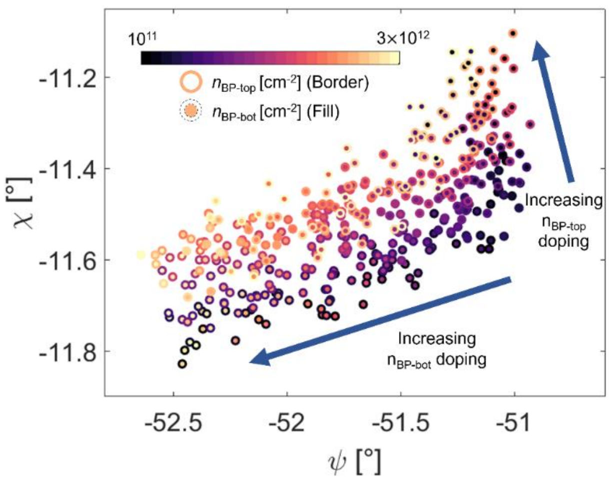

Fig. 5b:

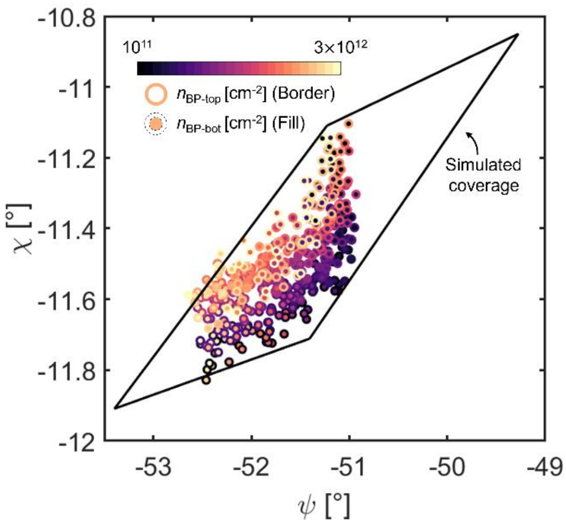

We also note that a third of the data scatter points were previously not properly plotted onto Fig. 4c and 5b. These data points were previously included in the table of supplementary note 7 but were not plotted due to a scripting error. This has now been corrected in Fig. 4c and 5b.

• The simulations in 2d and 2e show clear structure in the ellipse parameters which are not observed experimentally. Why is this? Can the non-idealities highlighted in the discussion explain the lack of topography?

The reviewer brings up an interesting question here regarding the structure in the ellipse parameters as a function of gating voltages. The simulation maps in Fig. 2c-e show the case where the critically coupled point can be accessed by an intermediate combination of both voltages. As mentioned in the main text, an optical phase singularity occurs at this point, which results in structure in the ellipse parameters. However, away from the singularity (e.g. bottom right region of Fig. 2c-e), both the anisotropic phase modulation and amplitude ratio modulation drops significantly, which result in just a gradient in the S_0, ψ and χ voltage maps. This is further illustrated in Supplementary Fig. 8d-f, where the PMMA layer has been reduced slightly from 490 nm to 470 nm, causing the critically coupled point to be inaccessible by gating. As such, only a gradient in the gating maps are observed. Similarly, since the fabricated device operates in the undercoupled regime, far from the critically coupled point, only a gradient can be seen in the voltage maps.

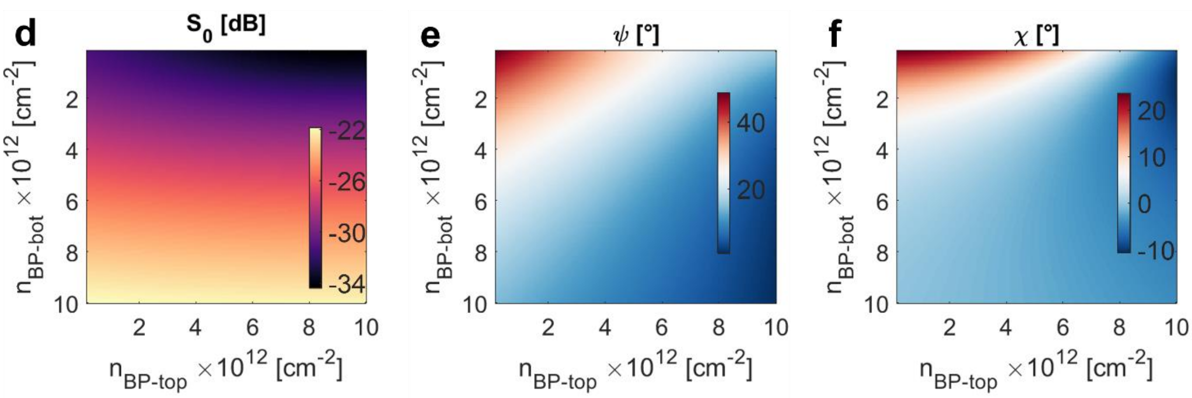

Supplementary Fig. 8. (**d-f**) S_0, azimuthal and elliptical maps as a function of top and bottom carrier densities, for a non-critically coupled case where the top PMMA layer is reduced from the optimal 490 nm to 470 nm.

• The authors only list the simulated Poincare sphere coverage in the abstract. Either the language should be weakened (aka simulations predict an 86% coverage), or the experimentally demonstrated percentages should be mentioned.

The reviewer brings up a relevant point on the listed Poincare sphere coverage. As such, we have modified the line in the abstract to read:

"Our heterostructure design predicts electronic access to 86% of the Poincaré sphere at its S-band operating wavelength."

• The objective has angular spread which muddles the input polarization state to the device. How much does this influence the simulated performance of the device? Can this explain some of the discrepancies between theory and experiment?

To address the reviewer's questions, we added the following analysis to supplementary note 15:

"While the objective lens does introduce some electric field energy into the longitudinal fields, the effect is expected to be small for our optical setup parameters. This can be explicitly evaluated using equation (3.66) in reference [15]. Here, we use NA = 0.4, and a moderate filling factor of $f_0 = 1$. By numerically solving the integrals for the electric field of the (0,0) mode, we find that for our objective, if linearly polarized light is launched along the E_x-direction, then

$$\frac{Max(E_y^2)}{Max(E_x^2)} = 6 \times 10^{-5}, \frac{Max(E_z^2)}{Max(E_x^2)} = 0.017$$

The amount of energy in the y-direction is significantly less than the precision error of tuning the rotatable half-waveplate that determines the input polarization angle into the device, indicating that focusing has a negligible effect on the in-plane polarization angle. The energy in E_z from focusing is expected to slightly smear out the reflectance spectra due to having a very narrow range of incident angles into the Fabry-Perot cavity. This may explain the slightly broader linewidth of the black curve in Fig. 5a compared to the simulated orange curve (which assumes purely plane-wave incident light). Nonetheless, at 1.7% energy in E_z compared to E_x, and at a NA of 0.4, this effect is expected to be significantly less than the discrepancies observed between the black (experiment) and dotted red curve (lossless cavity simulation) in Fig. 5a."

• Measurements were performed in reference to Au covered PMMA. What are the consequences of this in terms of the absolute reflectance measurements.

Reflectance plots in Fig. 3c were normalized against PMMA (460 nm) on gold (110 nm). The absolute reflectance measurements for the device, PMMA-covered gold reference, and the dark spectrum (taken with a beam block between objective and beam splitters) are plotted in Supplementary Fig. 14a for the 17° plot in Fig. 3c. Less than 0.01% reflectance variation is expected across the spectral measurement window for the PMMA-on-gold reference, as shown by transfer matrix calculations (Supplementary Fig. 14b).

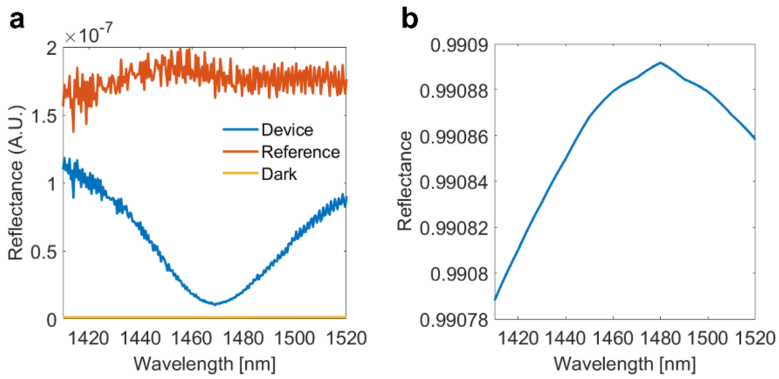

Supplementary Fig. 14. (**a**) Absolute reflectance measurements for the 17° plot in Fig. 3c, showing the device, PMMA-covered gold reference, and dark reflectances. (**b**) Transfer matrix model calculated reflectance of 460 nm PMMA on 110 nm gold.

• How much does the Poincare sphere coverage decrease if the input polarization is not at exactly 45 degrees to the two flakes?

This is an important question pertaining to input polarization angle sensitivity. We have prepared an analysis for both the critically coupled case, and non-critically coupled case, and added this analysis to supplementary note 8.

"In the critically coupled case, rotating the input polarization angle away from the AC axis of one of the BP layers reduces the tunability of the electric field along that direction. This results in a vertical or horizontal stretching of the S_0, ψ and χ voltage maps in Fig. 2c-e. For example, a 15° input relative to the bottom BP layer's AC-axis horizontally elongates the critically coupled point as the reflected light becomes less sensitive to modulations of the top BP layer (Supplementary Fig. 8a-c). This elongation also decreases the average optical efficiency of the device (Supplementary Fig. 8g), while decreasing the overall Poincare sphere coverage (Supplementary Fig. 8h). We note that the sharp drop off seen in Supplementary Fig. 8h occurs when significant features of the azimuthal and elliptical maps are cut off due to the large horizontal stretching at lower input angles. However, the coverage is relatively agnostic to input polarization in the 20-45° input range as the ellipse parameter singularity features are still largely accessible within the voltage parameter space.

Similar trends were observed in the non-critically coupled case, where the top PMMA layer thickness was reduced from the optimal 490 nm to 470 nm, causing the critically coupled point to be inaccessible through gating. However, in this case since the optical phase singularity is no longer accessible, horizontal stretching of the plot linearly reduces the polarization coverage instead (Supplementary Fig. 8i)."

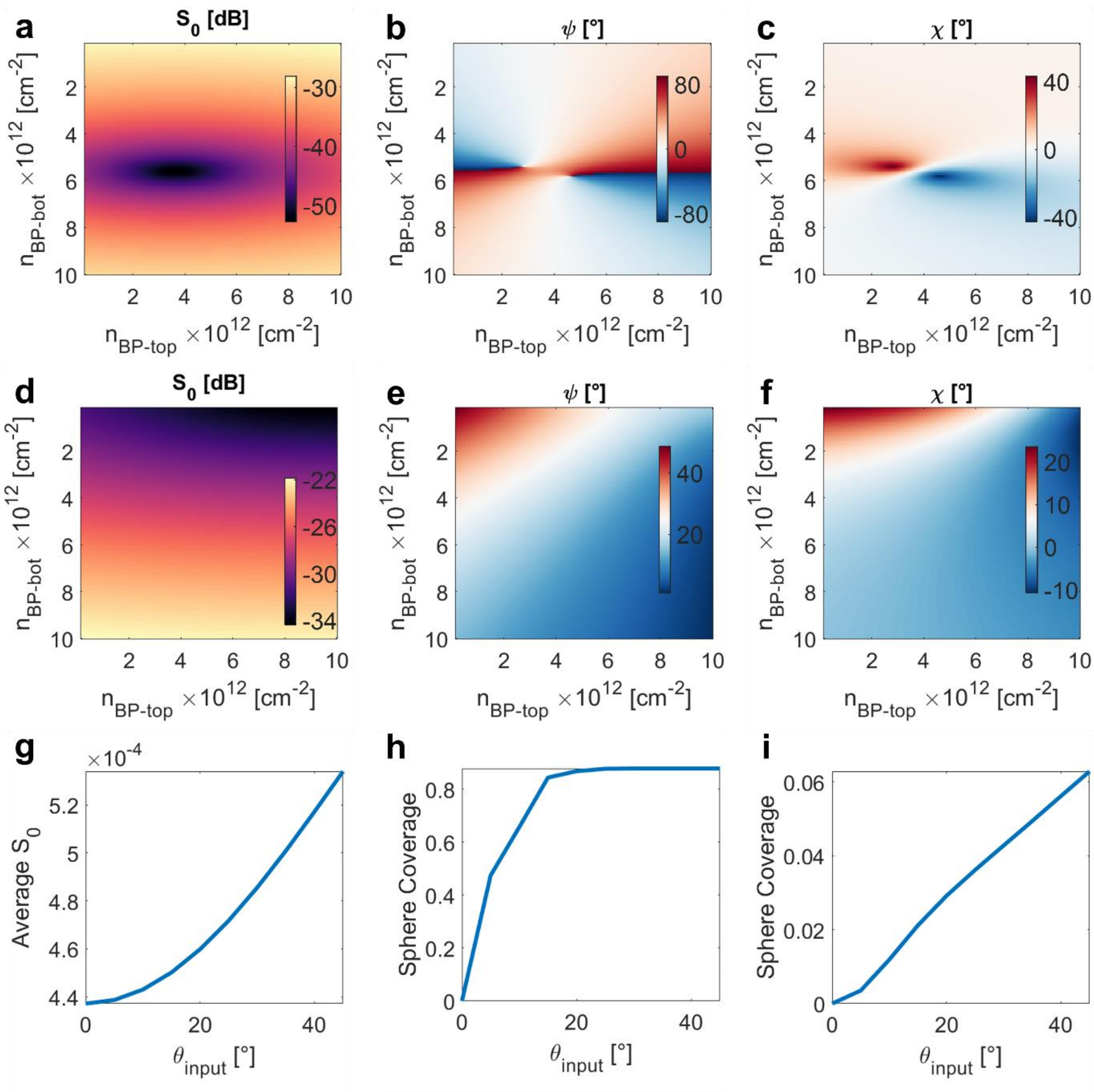

Supplementary Fig. 8. Effect of input polarization angle on polarization modulation. (**a-c**) S_0, azimuthal and elliptical maps as a function of top and bottom carrier densities, for the same device presented in Fig. 1 & 2, but with a 15° input polarization angle to the bottom BP flake's AC axis. (**d-f**) S_0, azimuthal and elliptical maps as a function of top and bottom carrier densities, for a non-critically coupled case where the top PMMA layer is reduced from the optimal 490 nm to 470 nm, and with a 15° input angle. (**g**) and (**h**) are the average S_0 and the total Poincare sphere coverage as a function of input polarization angle for the critically coupled case (a-c), while (**i**) shows the Poincare sphere coverage for the non-critically coupled case (d-f).

• How much depolarization is present in the measured experimental data?

We address this question by including the following into supplementary note 16:

"In Fig. 4c, the average degree of polarization across the data was measured to be

$$Mean\left(\frac{P_{pol}}{P_{pol}+P_{unpol}}\right) = 88.4\%$$

There are several sources expected to contribute to this. Firstly, the objective lens, the beam splitter and the tube lens in the setup are expected to cause some depolarization due to scattering. Secondly, the spatial variations across the sample (seen in Fig. 3d, e), combined with the finite beam radius at focus causes some degree of polarization variation. Lastly, while ambient light entering the polarimeter was minimized during experiments, it was not fully eliminated according to dark measurements performed where a beam block was placed between the objective and beam splitters. This was measured to account for about 7% out of the 11.6% depolarization at the resonance wavelength. As such, we do not expect significant depolarization from the polarization modulator itself."

Reviewer #3 (Remarks to the Author):

I co-reviewed this manuscript with one of the reviewers who provided the listed reports. This is part of the Nature Communications initiative to facilitate training in peer review and to provide appropriate recognition for Early Career Researchers who co-review manuscripts.

We thank the reviewer for their time, comments and insight in improving the work.

Reviewer #4 (Remarks to the Author):

The manuscript reports a dual-gated, Fabry-Perot cavity device integrating two orthogonally aligned black phosphorus (BP) layers. The authors demonstrate the ability to independently control two degrees of freedom (azimuthal and ellipticity angles) via electrical gating, thereby accessing a significant portion of the Poincaré sphere, at a fixed telecommunication wavelength.

The concept of twisted BP layers for full polarization control has been theoretically explored in Ref. 27. Here, this manuscript provides further experimental validation of a dual-gated, twisted BP device in a metal-mirror Fabry-Perot cavity configuration. The manuscript is generally well-written, and relevant references are properly cited. However, my primary concern is that the experimentally realized range of polarization modulation appears quite limited, falling significantly short of the simulation predictions. Nevertheless, the demonstration of a "2D-control" device based on van der Waals heterostructures remains a notable contribution to the field. I suggest that the authors address the following issues:

We thank the reviewer for their time and feedback on the manuscript. We address the issues below accordingly, with the concern on experimental modulation falling short of simulation predictions addressed in the responses to questions 2 and 4.

1.In the simulations presented in Fig. 1, the accessible polarization coverage is stated to be 86%. However, in Figure 5c, assuming an optimized top gold mirror thickness, the simulated coverage drops to 70%. What is the reason for this discrepancy?

In Fig. 5c, intracavity losses were introduced into the model to account for heterostructure imperfections and match the transfer matrix model to the experimental reflectance results. These additional losses, modelled as a distributed loss through the cavity by increasing the imaginary refractive index of the hBN dielectric, effectively reduce the Q of the device. This firstly leads to reduced phase buildup within the cavity. Secondly, the increased reflectance linewidth results in a reduction in anisotropic amplitude ratio modulation under gating. Combined, the reduced device Q therefore causes the total Poincare sphere coverage to drop. We demonstrate this by performing intermediate simulations at various k_{hBN} values, and summarized the results in supplementary note 10.

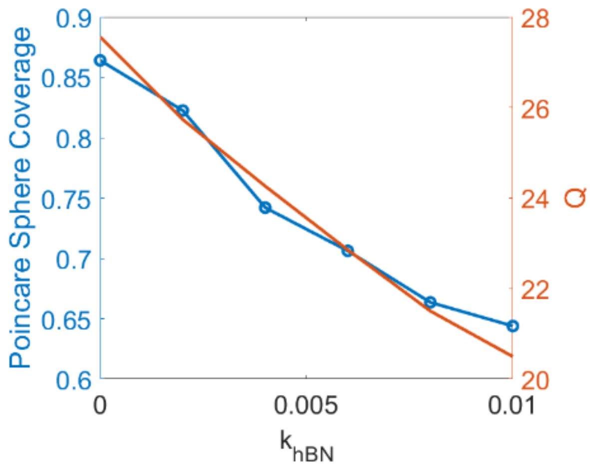

Supplementary Fig. 10. Simulated Poincare sphere coverage and cavity Q as a function of intracavity loss (modelled by increasing the imaginary part of the hBN dielectric). The reduction in Q reduces the anisotropic amplitude ratio modulation and phase modulation of the device, which causes total coverage to drop

To clarify this discrepancy, the above figure and explanation is included in Supplementary note 10, and the following was added to the final paragraph of the discussions section:

"Further analysis on the Poincare sphere coverage as a function of cavity loss is included in supplementary note 10."

2.The authors only provide the coverage range of Poincaré sphere for the simulations; what is the specific polarization coverage percentage achieved in the actual experiments? Furthermore, in Fig. 5b, there appears to be a significant deviation between the experimental data and the simulated range (15.5 nm top gold mirror thickness). The manuscript lacks a specific analysis for this discrepancy.

Firstly, we note that a correction where a third of the data scatter points were previously not plotted onto Fig. 4c and 5b. These data points were previously included in the table of supplementary note 7 but were not plotted due to a scripting error. This has now been corrected in Fig. 4c and 5b.

Corrected Fig. 5b:

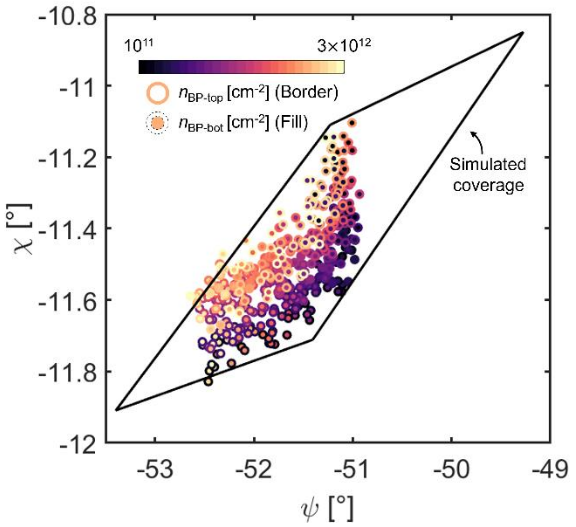

The specific polarization coverage achieved in experiments was 0.007%, with the remaining discrepancy between simulation and experiments in Fig. 5b possibly stemming from imperfect gold evaporation, inefficient contacts, or mobility-hindered excitons.

Firstly, we note the sensitivity of the device to the thickness of the top gold layer. Supplementary Fig. 11 shows the simulated Poincare sphere coverage for the device in Fig. 1, as a function of gold thickness. As the polarization modulation is maximized at critical coupling, the coverage is significantly affected by gold thickness at the angstrom level, with coverage dropping below 5% for gold that is >1 nm off in thickness. In practice, it is difficult to achieve angstrom-accurate gold deposition, especially without knowing the intracavity heterostructure losses *a priori*. The AFM measurement of the deposited gold (which is fed into the simulations) also has a sensitivity limit of a few angstroms, possibly explaining the discrepancy in Fig. 5b.

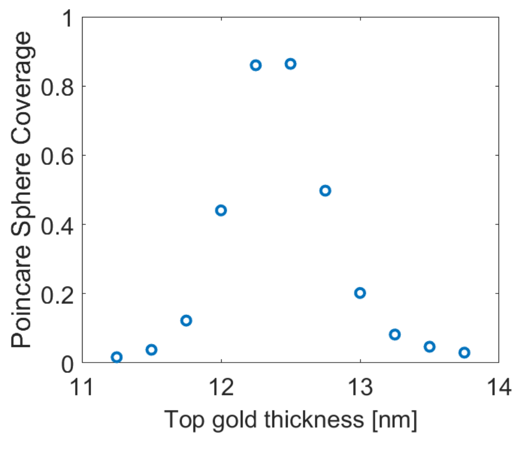

Supplementary Fig. 11. Simulated Poincare sphere coverage as a function of top gold thickness for the device in Fig. 1 and 2, showing optimal coverage at a thickness of ≈12.5 nm. 1 nm away from the optimal thickness, the coverage drops below 5%.

The sensitivity of the device to the top gold layer also underpins the importance on the gold deposition quality. At these small thicknesses, evaporator conditions heavily influence the crystallinity of the deposited gold. There is a need to properly seed the gold layer to avoid island-like growth as seen in reference [16]. For our fabrication, the gold layer was seeded with 1 nm of Ti, but no optimization studies were done to determine the dependence of gold roughness on the seeding layer for a hBN substrate. We recognize this as a potential subject for further studies to improve the overall Poincare sphere coverage.

Other possible reasons for the discrepancy relate to the simple capacitance model for estimating carrier concentrations and exciton oscillator strength as a function of gating voltage. The model neglects effects such as inefficiencies in the gold contacts and interconnects due to resistance, and the quantum capacitance of the BP layer.[17,18] Furthermore, defects within the BP layers are expected to locally trap excitons[19], while exciton-phonon interactions can limit exciton mobility.[20] These effects could potentially reduce the exciton oscillator strength dependence on carrier density.

We also note several methods to further extend polarization coverage in experiment. For example, we only gated up to a third of the voltage before the dielectric breakdown limit to preserve the device for additional testing, as opposed to simulations where the carrier density was 3 times higher. This was in anticipation of having pinholes in the hBN layers that would reduce the breakdown limit below 0.5 V/nm. Nonetheless, the device had not yet seen significant leakage current at the current doping levels and could be pushed further in experiment.

The above analysis has been included in supplementary note 11, with the following added to the main text in the discussions section:

"The discrepancy between the simulated coverage and experimental data are attributed to device non-idealities, and are further expounded upon in supplementary note 11."

3.The device utilizes metal for contacts/mirrors. How do the losses of metal layers influence the modulation of the polarization states?

The reviewer brings up an interesting question regarding metal losses and polarization modulation. From a cavity standpoint, we expect the losses from the gold mirrors to reduce the cavity Q and therefore reduce the Poincare sphere coverage. This analysis has been added into the manuscript as supplementary note 10. For maximal modulation, losses should ideally only stem from the BP layer where anisotropic phase pickup and excitonic absorption occurs.

At present, we measured the cavity loss rate $\kappa \approx 59$ meV, and the exciton decay rate $\gamma \approx 50$ meV. This indicates that the use of a non-lossy mirror would significantly enhance the modulation range, while maintaining relatively high optical efficiencies. In Ref. [9], the gold mirrors were replaced with distributed Bragg reflector stacks, enabling the operating wavelength to be detuned away from the excitonic resonance of the BP layers to improve the amount of phase and amplitude modulation per unit loss. As a result, the design predicts electronic access over more than 90% of the Poincare sphere. Here, gold mirrors were used for ease of fabrication to demonstrate the concept of two-parameter control using a 2D heterostructure, even though it inevitably limits the optical efficiency and polarization coverage of the device.

We have added the following to the 2nd last paragraph of the discussions section:

"Further analysis on the Poincare sphere coverage as a function of cavity loss is included in supplementary note 10."

We have also added the following sentence to paragraph 2 of the results section:

"We also note that the optical modulation efficiency reported here is fundamentally limited by the lossy gold mirrors of the Fabry-Perot cavity, but can be improved by replacing them with distributed Bragg reflector mirrors instead as reported in [29]."

4.The authors mention that the fabrication process introduces numerous imperfections and contamination, a challenge that is compounded in a 5-stack heterostructure. Given the stochastic nature of the fabrication and the small size of the usable active area, is the reported result reproducible across different devices?

The reviewer brings up an important question regarding the reproducibility of many-layer, complex heterostructure stacks. Multi-layer heterostructure stack fabrication has been shown to be repeatable in numerous studies. In particular, we cite references where complex 4-6 layer heterostructure stacks, some including twisted flakes, have shown reproducible results.[4,21,22]

To explicitly show reproducibility of the results for our device design, we took efforts to fabricate an additional device, with the results summarized in Supplementary Fig. 9. The micrograph of the device is shown in Supplementary Fig. 9a, together with the Raman measurement results of the BP flakes and the input polarization angle (55° to the horizontal). The passive spectral polarization tuning is summarized in Supplementary Fig. 9b, showing a reflectance minima of 1.5% due to a more accurate thickness of gold being deposited. Two-parameter polarization control is demonstrated with the new device, showing dependence of both ellipse parameters on both the top and bottom gating voltages (Supplementary Fig. 9c-e).

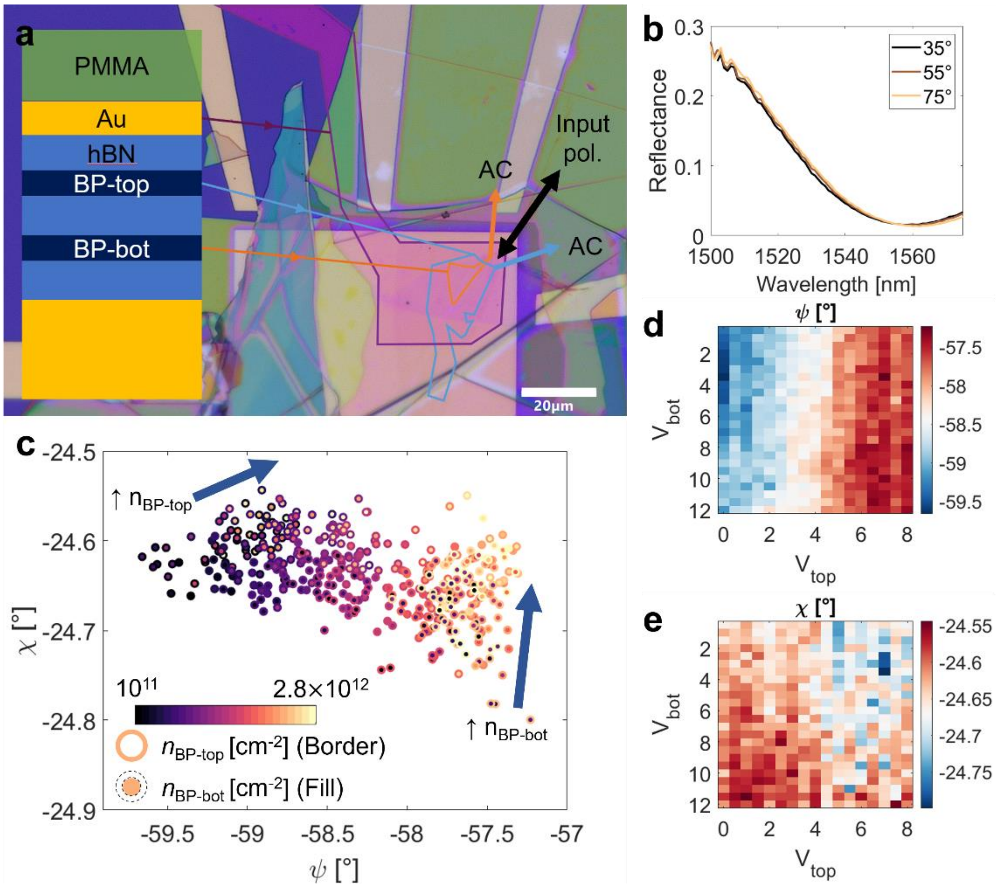

Supplementary Fig. 9. Fabrication and experimental results of the second dual-gated BP device. (**a**) Optical image of the device, with the top gold mirror, top BP layer and bottom BP layer outlined in purple, blue and orange respectively. Inset shows the cross-sectional schematic. The top BP layer makes electrical contact with the north-eastern gold finger, while the bottom BP layer is contacted by the eastern gold finger. The AC axis separation of the two BP layers was determined to be 66°. The black double headed arrow marks the input polarization angle of 55° used in subsequent measurements. White scale bar represents 20μm. (**b**) Normalized reflectance of the device at different input polarization angles, showing a 1.5% minimum at 1561nm. (**c**) Normalized Poincare sphere plot showing 2D polarization coverage over Poincare sphere. The top (bottom) BP doping density is represented in border (fill) color of the plot points (from black to peach). (**d** and **e**) Measured azimuthal and elliptical coordinate as a function of top and bottom gating.

Overall, the device, while being marginally better coupled, has a smaller active area (owing to a smaller 3L-BP bottom flake), is more detuned away from the exciton resonance wavelength (due to a thicker cavity), has poorer AC-axes alignment (66° separation), and has a smaller spectral overlap between the top and bottom BP flakes (due to imperfect top and bottom hBN flake thicknesses). This resulted in a Poincare sphere coverage that was about 60% less than the original device in Fig. 3-5.

Nonetheless, we note that none of the above factors fundamentally precludes the possibility of a device spanning a larger polarization coverage range. Using cleaner pickup and transfer techniques[23], performing Raman microscopy within the glovebox to determine BP crystallographic direction before stacking, more precise and judicious selection for hBN flake thickness, careful seeding of the top gold layer to minimize mirror roughness, and exfoliating larger 3L-BP flakes than those used in this work are but some ways in which device fabrication could be improved. Here, we propose and demonstrate a new way of electronic polarization modulation via two-parameter control. While an optimal device fabrication remains difficult owing to its sensitivity to many different factors (top gold thickness, size and quality of flakes, alignment of BP flakes, thickness of each of the 5-layers, cleanliness of sample), we show proof of concept of this 2D control with varying degrees of polarization coverage.

We add the above results and analysis to supplementary note 9, and include the following sentence at the end of the results section:

"An additional device was also fabricated to show reproducibility of the two-parameter tuning results (see supplementary note 9)."

5.What is the modulation speed of the device?

The fabricated devices were unfortunately RC-limited since the contacts and interconnects were not optimized for low resistance or parasitic capacitance. Proper circuit modelling and design work is required before high-speed AC voltages can be applied to the device. Furthermore, the source meter used for gating exhibits large voltage overshoots when stepping the voltage, which greatly increase the risk for device breakdown under fast modulation. Since the goal of the study was to observe two-parameter control in 2D heterostructures in the steady state, we therefore opted to not subject the device to AC voltages.

Nonetheless, we note several other studies measuring the rise and fall time of BP at the nanosecond scale.[24-26] The studies demonstrate the high responsivity and exciton mobility of BP under optimal electronic considerations. We therefore do not expect a fundamental physical limitation to the modulation speed of the device given these studies.

We have added the new references to the 2nd paragraph of the introduction ([18] & [19] in the revised manuscript), and also added the following sentence to the 2nd last paragraph of the discussions:

"Further improvements to the device's circuit design to minimize resistance and parasitic capacitance for high-speed modulation are possible, but remain beyond the scope of this work (see [17-19] for ns-scale rise and fall times in BP)."

6.The visualization of the polarization state evolution in Fig. 4c and Fig. 5b is somewhat unclear. Are these intended to be three-dimensional plots? A clearer representation would be beneficial.

We fully agree with the reviewer that the plots could be improved. We decided to modify Fig. 4c and 5b by doing 2-dimensional scatter plots in the ellipse parameter space instead for clarity.

Fig. 4c:

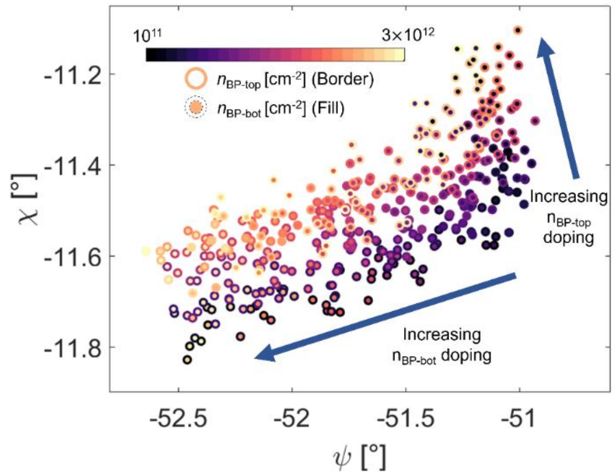

Fig. 5b:

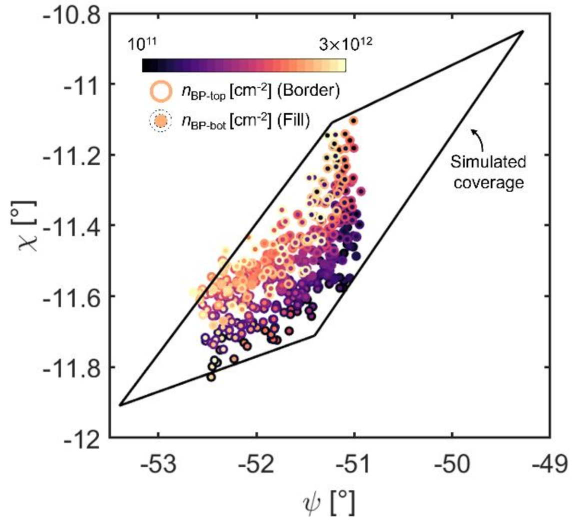

References:

1. Nguyen, P. V.; Teutsch, N. C.; Wilson, N. P.; Kahn, J.; Xia, X.; Graham, A. J.; Kandyba, V.; Giampietri, A.; Barinov, A.; Constantinescu, G. C.; Yeung, N.; Hine, N. D. M.; Xu, X.; Cobden, D. H.; Wilson, N. R. Visualizing electrostatic gating effects in two-dimensional heterostructures. *Nature* **2019**, 572, 220-223.
2. Li, M.; Biswas, S.; Hail, C. U.; Atwater, H. A. Refractive Index Modulation in Monolayer Molybdenum Diselenide. *Nano. Lett.* **2021**, 21(18), 7602-7608.
3. Weintrub, B. I.; Hsieh, Y. L.; Kovalchuk, S.; Kirchhof, J. N.; Greben, K.; Bolotin, K. I. Generating intense electric fields in 2D materials by dual ionic gating. *Nat. Comm.* **2022**, 13:6601.
4. Xiong, Y.; Wang, Y.; Zhu, R.; Xu, H.; Wu, C.; Chen, J.; Ma, Y.; Liu, Y.; Chen, Y.; Watanabe, K.; Taniguchi, T.; Shi, M.; Chen, X.; Lu, Y.; Zhan, P.; Hao, Y.; Xu, F. Twisted Black Phosphorus–based van der Waals Stacks for Fiber-integrated Polarimeters. *Sci. Adv*. **2022**, 8, eabo0375.
5. Chen, S.; Liang, Z.; Miao, J.; Yu, X. L.; Wang, S.; Zhang, Y.; Wang, H.; Wang, Y.; Cheng, C.; Long, G.; Wang, T.; Wang, L.; Zhang H.; Chen, X. Infrared optoelectronics in twisted black phosphorus. *Nat. Comm*. **2024**, 15:8834
6. Wang, S. Y.; Li, D. K.; Zha, M. J.; Yan, X. Q.; Liu, Z.; Tian, J. Tunable Optical Activity in Twisted Anisotropic Two-Dimensional Materials. *ACS Nano* **2023**, 17(16), 16230-16238.

7. Higashitarumizu, N.; Tajima, S.; Kim, J.; Cai, M.; Javey, A. Long operating lifetime mid-infrared LEDs based on black phosphorus. *Nat. Comm.* **2023**, 14:4845.
8. Park, J.; Jeong, B. G.; Kim, S. I.; Lee, D; Kim, J; Shin, C; Lee, C. B.; Otsuka, T; Kyoung, J.; Kim, S.; Yang, K. Y.; Park, Y. Y.; Lee, J.; Hwang, I.; Jang, J.; Song, S. H.; Brongersma, M. L.; Ha, K.; Hwang, S. W.; Choo, H.; Choi, B. L. All-solid-state spatial light modulator with independent phase and amplitude control for three-dimensional LiDAR applications. *Nat. Nano*. **2021**, 16, 69-76
9. Seah, S. K. W.; Biswas, S.; Hail, C. U.; Jang, M. S.; Atwater, H. A. Efficient, Polarization-Diverse State Generation with Tunable Black Phosphorus Cavity Heterostructures and Active Metasurfaces. *ACS Photonics* **2025**, 12(3), 1409-1417.
10. Schneider, C.; Glazov, M. M.; Korn, T.; Höfling , S.; Urbaszek, B. Two-dimensional semiconductors in the regime of strong light-matter coupling. *Nat. Comm*. **2018**, 9:2695.
11. Chikkaraddy, R.; de Nijs, B.; Benz, F.; Barrow, S. J.; Scherman O. A.; Rosta, E.; Demetriadou, A.; Fox, P.; Hess, O.; Baumberg, J. J. Single-molecule strong coupling at room temperature in plasmonic nanocavities. *Nature* **2016**, 535, 127–130.
12. Chen, Y.; Quek, S. U. Tunable bright interlayer excitons in few-layer black phosphorus based van der Waals heterostructures. *2D Mater.* **2018**, 5(4), 045031.
13. Biswas, S.; Wong, J.; Pokawanvit, S.; Yang, W. C. D.; Zhang, H.; Akbari, H.; Watanabe, K.; Taniguchi, T.; Davydov, A. V.; Jornada, F. H.; Atwater, H. A. Edge-Confined Excitons in Monolayer Black Phosphorus. *ACS Nano* **2023**, 17(23), 23692-23701.
14. Datta, I.; Chae, S. H.; Bhatt, G. R.; Tadayon, M. A.; Li, B.; Yu, Y.; Park, C.; Park, J.; Cao, L.; Basov, D. N.; Hone, J.; Lipson, M. Low-loss Composite Photonic Platform Based on 2D Semiconductor Monolayers. *Nat. Photonics* **2020**, 14, 256-262.
15. Novotny, L; Hecht, B. Propagation and focusing of optical fields. In: Principles of Nano-Optics. Cambridge University Press **2012**, 45-85.
16. Maniyara, R. A.; Rodrigo, D.; Yu, R.; Canet-Ferrer, J.; Ghosh, D. S.; Yongsunthon, R.; Baker, D. E.; Rezikyan, A.; Abajo, F. J. G.; Pruneri, V. Tunable plasmons in ultrathin metal films. *Nat. Photonics* **2019**, 13, 328-333.
17. Bennett, R. K. A.; Pop, E. How Do Quantum Effects Influence the Capacitance and Carrier Density of Monolayer MoS2 Transistors? *Nano Lett.* **2023**, 23(5), 1666-1672.
18. Awate, S. S.; Mostek, B.; Kumari, S.; Dong, C.; Robinson, J. A.; Xu, K.; Fullerton-Shirey, S. K. Impact of Large Gate Voltages and Ultrathin Polymer Electrolytes on Carrier Density in Electric-Double-Layer-Gated Two-Dimensional Crystal Transistors. *ACS Appl. Mater. Interfaces* **2023**, 15(12), 15785-15796.
19. Wu, K.; Zhong, H.; Guo, Q.; Tang, J.; Yang, Z.; Qian, L.; Yuan, S.; Zhang, S.; Xu, H. Revealing the Competition between Defect-Trapped Exciton and Band-Edge Exciton Photoluminescence in Monolayer Hexagonal WS2. *Adv. Opt. Mater*. **2022**, 10, 2101971.
20. Tian, X.; Zheng, Q.; Jiang, X.; Zhao, J. Ab initio investigation on exciton-phonon interaction and exciton mobility in black phosphorene. *Phys. Rev. B* **2023**, 108, 245118.
21. Ciarrocchi, A.; Unuchek, D.; Avsar, A.; Watanabe, K.; Taniguchi, T.; Kis, A. Polarization switching and electrical control of interlayer excitons in two-dimensional van der Waals heterostructures. *Nat. Photonics* **2019**, 13, 131-136.
22. Khelifa, R.; Back, P.; Flöry, N.; Nashashibi, S.; Malchow, K.; Taniguchi, T.; Watanabe, K.; Jain, A.; Novotny, L. Coupling Interlayer Excitons to Whispering Gallery Modes in van der Waals Heterostructures. *Nano Lett*. **2020**, 20(8), 6155-6161.
23. Liu, H.; Zhao, J.; Ly, T. H. Clean Transfer of Two-Dimensional Materials: A Comprehensive Review. *ACS Nano* **2024**, 18(18), 11573-11597.
24. Youngblood, N.; Chen, C.; Koester, S. J.; Li, M. Waveguide-integrated Black Phosphorus Photodetector with High Responsivity and Low Dark Current. *Nat. Photonics* **2015**, 9, 247–252.
25. Chang, T. Y.; Chen, P. L.; Yan, J. H.; Li, W. Q.; Zhang, Y. Y.; Luo, D. I.; Li, J. X.; Huang, K. P.; Liu, C. H. Ultra-Broadband, High Speed, and High-Quantum-Efficiency Photodetectors Based on Black Phosphorus. *ACS Appl. Mater. Interfaces* **2020**, 12(1), 1201-1209.
26. Zhang, X.; Dai, M.; Wang, C. W.; Zhang, Y.; Zhu, S.; Wang, Q. J. Resonance-Enhanced Black Phosphorus Mid-Infrared Photodiode with Nanosecond Response and High Responsivity at Room Temperature. *ACS Nano* **2026**, 20(8), 7069-7078.
27. Wang, S.Y.; Huang, K.X.; Guo, Q.Q.; Guo, H.W.; Tian, J.G.; Liu, Z.B. Tunable Optical Rotation in Twisted Black Phosphorus. *J. Phys. Chem. Lett*. **2021**, 12, 4755-4761.
28. Biswas, S., Grajower, M. Y., Watanabe, K., Taniguchi, T., Atwater, H. A., Broadband Electro-optic Polarization Conversion with Atomically Thin Black Phosphorus. *Science* **2021**, 374, 448-453.
29. Ahmad, H.; Lim, H.S.; MatJafri, M.Z.; Ge, Y.Q.; Zhang, H.; Tiu, Z.C. All-fiber optical polarization modulation system using MoS2 as modulator. *Infrared Phys. Tech*. **2019**, 102, 103002.